J. Mater. Eng. (1987) 9:237–251

The Influence of Inclusion Chemical Composition on Weld Metal Microstructure

S. Liu and D. L. Olson

Abstract. The effects of nonmetallic inclusions on weld metal microstructures were investigated. The inclusions were extracted from niobium microalloyed steel weld metal specimens, and examined with light and electron microscopic techniques. An EDS (Energy Dispensive Spectroscopy) system was used to determine the chemical composition of the inclusions. Correlation between weld metal and inclusion composition was established. Aluminum, titanium, sulfur, and iron were the most important elements in the inclusions that affect the final weld metal microstructure. Mn/Si ratio was also found to affect the amount of oxygen and acicular ferrite in the weld. The state of deoxidation, as indicated by the amount of FeO present in the inclusions, actually determines the recovery of alloying elements and the amount of oxygen in the weld pool. It also determines the chemical composition of the nonmetallic inclusions. Inclusions with high aluminum content tend to cluster together forming larger particles while pure silica or silicate particles are small and well disseminated in the weld metal. This explains the different inclusion size distributions observed in the weld specimens of different oxygen concentration. Consequently, the prior austenite grain size will be different resulting in different amounts of acicular ferrite and grain boundary ferrite.

INCLUSION FORMATION

Weld Pool Deoxidation Reactions

In steelmaking, deoxidation is generally accomplished by adding chemical elements with higher affinity for oxygen than iron to the molten bath. For this reason, the remnant FeO is the melt may be used as an indicator of the degree of deoxidation of the steel. Deoxidation products can be classified as primary and secondary according to the temperature at which the deoxidation reactions occur. When deoxidation occurs at high temperature, at the moment when deoxidizing elements are added to the melt, the resulting product is termed primary. However, secondary deoxidation may also occur during the cooling of both liquid and solid steel at lower temperatures (due to the action of the alloying elements and the decreasing solubility of oxygen). Primary deoxidation products are generally easier to eliminate than the secondary ones. Lower temperature, lower mobility of the chemical species due to partial solidification, and weaker metal pool convection are the major factors of the entrapment of these secondary products. The solubility of oxygen in pure liquid iron is approximately 1600 ppm at the melting point [1,2]. On solidification, this decreases markedly and is only about 860 ppm at 1500° C in delta iron [1,2]. In addition to the low intrinsic solubility of oxygen in iron, most of the alloying elements present in liquid steel will further lower the solubility of oxygen, such that the actual concentration of oxygen in the metal pool is lower than those mentioned above. During the solidification process, the excess oxygen is rejected from solution and combines with the alloying elements present such as manganese, silicon, aluminum, titanium, etc., to form inclusions. The commonly used deoxidizing elements in steel melts are manganese, silicon, aluminum, and silicon–manganese alloys. Titanium, zirconium, calcium, and rare earth metals are less commonly used. In submerged-arc welding of steels, these elements may come from the base metal, the electrode welding wire, and the welding flux.

S. Liu and D.L. Olson are with the Center for Welding Research Dept. of Metallurgical and Materials Engineering, Colorado School of Mines, Golden, CO 80401.

In normal conditions of weld pool deoxidation by silicon, the only product that can exist is the solid silica SiO_2 [1,2]. With high oxygen concentration and low silicon content in the weld pool, liquid iron silicate FeO–SiO_2 (faialite) may also be formed. Using manganese as the only deoxidant in the system, the final inclusion can be both solid and liquid MnO and will contain a small amount of FeO [1–3]. This suggests that the inclusion composition will depend on the manganese level, the MnO activity, in the molten bath. The shape of the oxide inclusions depends on the MnO/FeO ratio [3]. Those containing a high proportion of FeO are usually spherical, whereas the morphology becomes increasingly irregular as MnO increases.

Sometimes, aluminum is used alone as deoxidant and the possible inclusions at 1600° C are FeO–$Al_2O_{3(l)}$, FeO–$Al_2O_{3(s)}$ (known as hercynite), or Al_2O_3 (corundum) [1–3]. The formation of pure aluminum oxide, however, is favorable only in high aluminum content melts.

Phase relations among oxides formed when titanium is used as deoxidizer in steel are very complicated. In the order of increasing titanium oxide (i.e., increasing amount of titanium used as deoxidizer), the intermediate phases likely to be present in the inclusions could be FeO, 2FeO–TiO_2, FeO–TiO_2 (Ilmenite), FeO–2TiO_2, and TiO_2 (rutile). Ti_3O_5, Ti_2O_3 and TiO can also be present as inclusions in a steel weldment.

No intermediate compounds are formed between FeO and ZrO_2 and a mixture of the two phases, wustite and zirconia, will result.

The relationship between the concentrations of oxygen and deoxidants in solution in iron in equilibrium with their respective pure oxides at 1600° C [2] are shown in Figure 1, which indicates the effectiveness of deoxidation of each one of the elements.

However, in steelmaking practices (furnace deoxidation or ladle deoxidation) or in welding processes, usually more than one deoxidant is used. When several deoxidants are present in the system, the product will be inclusions composed of duplex or more complex oxides in which each oxide may have its thermodynamic activity lower than one. It is easy to determine that the deoxidizing power of silicon is increased if a_{SiO_2} is less than one. Therefore, simultaneous deoxidation by manganese and silicon, or combination of other elements, gives much lower residual oxygen in solution because of the reduced silica activity. It is possible to form a liquid product of low silica activity containing some FeO. In the case of low silicon, high manganese and aluminum content, MnO can react with Al_2O_3 forming a solid compound known as Galaxite (MnO–Al_2O_3) [1–3]. FeO may substitute the MnO in the galaxite forming a continuous series of solid solution from galaxite to hercynite. The final form will be (FeO,MnO)–Al_2O_3. More commonly, manganese, silicon, and aluminum are present together in the molten pool and the compositions of the resultant inclusions might be satisfactorily represented, as a first approximation, in terms of the quaternary system FeO–MnO–Al_2O_3–SiO_2. This is closest to the welding situation.

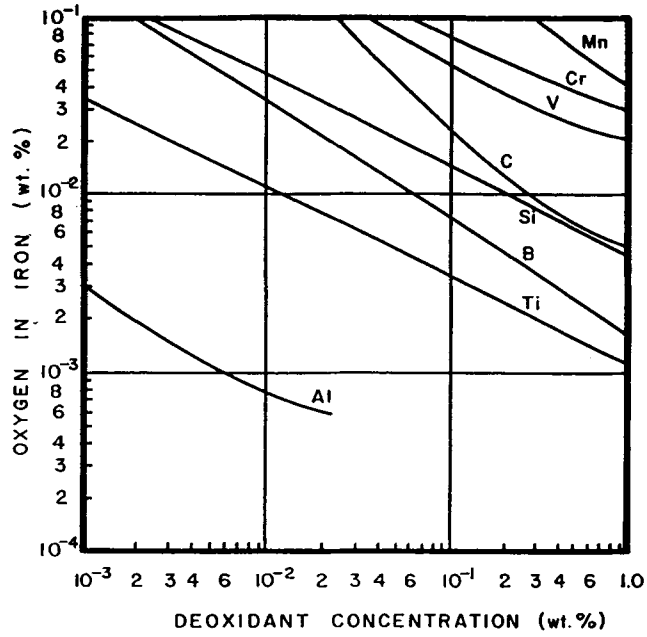

Fig. 1. Relationship between the concentrations of oxygen and deoxidants in molten iron in equilibrium with their respective pure oxides at 1600° C. [2]

Inclusion Entrapment

The removal of the deoxidation products is important in assuring a low oxygen cast or weld after solidification. The rate of rise (floating) of a reaction product phase is given by Stoke's equation [1–2],

$$\dot{r} = \frac{2}{9} \cdot g \cdot r^2 \cdot \left(\frac{\rho_{liq} - \rho_{particle}}{\eta} \right) \qquad (1)$$

where $\dot{r}$ = rate of rise (floating) in 10^{-2} m/s
g = gravitational constant (9.80 m/s^2)
r = radius of the rising particle (10^{-2} m)
ρ = density
η = viscosity of the liquid melt

In steelmaking practices, the holding time for deoxidation is usually limited to under 20 min (because of the enormous heat loss in the ladle) [1–2]. This allows time for particles of diameter larger than 0.2 mm diameter to clear the solution, and particles smaller than

that would be entrapped in the melt. Particles of sizes smaller than 0.01 mm will not be eliminated even after the refining stage [1–2]. From Eq. (1), a larger difference in densities between inclusion and liquid results in a faster floating rate and more effective separation of the inclusions from the melt. A similar effect is observed in larger size particles. This is due to the larger buoyancy force exerted by the liquid on larger size inclusions. Therefore, the number of particles and the growth and rise of the particles in the bath are important factors in obtaining a "clean" metal. The three basic steps involved in the deoxidation reactions are:

(a) formation of critical nuclei of the deoxidation products, (b) progress of deoxidation resulting in growth of the reaction prducts, and (c) flotation of the products from the melt. The nucleation rate is exponentially proportional to the free energy barrier to nucleation, which by its turn, is essentially a function of the metal oxide/metal interfacial energy and the volume free energy change of the deoxidation reaction. Following nucleation, there are four mechanisms [4] for the growth of a stable nucleus, namely Brownian movement, Ostwald ripening, solute diffusion, and particles collision. The growth of a particle from the size of a nucleus (a few Angstroms) to that of a particle of some intermediate size (tenths of a micron to a few microns) can be explained by solute diffusion. Further growth must involve collision of particles which depend on the convective movement of the bath and the velocity of the colliding particles [4]. However, growth processes are usually slow, requiring some finite periods of time for the reaction to complete. In welding, particularly, the very high temperature in the weld pool, the moving heat source, and the rapid cooling and solidification of the molten metal contribute to even higher possibility of inclusion entrapment, in spite of the large turbulence in the weld pool (compared to the refining stage in steelmaking processes).

Grong, Siewert, Martins and Olson [5] investigated the silicon–manganese deoxidation of steel weld metals and determined that under dynamic conditions such as those found in a weld pool, buoyancy effect does not play a significant role in the separation of oxide inclusions. Fluid flow pattern is the controlling factor of inclusion distribution. For particles within the typical size range of weld metal inclusions (less than 2.0 μm in diameter), the drag force due to liquid metal flow velocity is orders of magnitude greater than the other forces acting on these particles. They also suggested that inclusions formed in the hot, turbulent part of the weld pool are brought immediately to the upper surface behind the arc. In gas metal-arc welding (GMAW), this results in the formation of a thin layer of slag covering the weld bead. While at a slightly lower temperature, the inclusions formed in the cooler part of the weld will be trapped.

Hannerz and Werlefors [6] examined the inclusions in welds of high manganese content made with highly basic fluxes. They observed that aluminum affects the size distributions of the inclusions. Probably as a result of a higher temperature of nucleation of aluminum slags (due to the higher aluminum concentration), the inclusions will have longer times to coalesce before solidification of the weld metal, resulting in larger entrapped inclusions. The same authors [6] concluded that the coarsening of the distribution is sufficient to explain the observed drop in notch toughness. However, an earlier nucleation will also favor the removal of inclusions by the top slag which will result in a lower oxygen content improving the weld metal toughness.

Types of Inclusions Commonly Encountered in Microalloyed Steels and Weld Metals

The chemical elements contained in microalloyed steels and the most common precipitates and nonmetallic inclusions such as oxides, silicates, aluminates, sulfides, and oxy-sulfides are summarized in Table I [7–12]. In terms of chemical composition, the inclusions found in microalloyed steel weld metal are not too different from those in the base metal. Ahlblom et al. [13] classified these inclusions into six groups:

1. $MnO + MnO–SiO_2$
2. $MnO–SiO_2 + Al_2O_3$; $MnO + Al_2O_3$; Al_2O_3
3. $MnS + SiO_2$
4. $MnS + Al_2O_3$; $MnS + SiO_2 + Al_2O_3$
5. MnS
6. Others

In the order of increasing aluminum addition to a low carbon steel weld pool which contains "mainly" manganese and silicon as deoxidants, the inclusions will be [14]:

1. $2MnO–SiO_2$
2. $MnO–SiO_2–Al_2O_3$
3. $MnO–Al_2O_3$
4. Al_2O_3

Increasing the weld metal titanium concentration, titanium content in the inclusions is also observed to increase, in the form of TiO_2 or TiO.

The main objective of this investigation is to examine in more detail the effects of nonmetallic inclusions on solid state phase transformations in steel weld metal, more specifically, to clarify how inclusion chemical composition can be related to the deoxidation practice and how that would influence the mechanisms of the austenite-to-ferrite transformation.

Table I. Summary of the Nonmetallic Inclusions Most Commonly Found in HSLA Steels [7–12]

Element	Carbide	Nitride	Nonmetallic Inclusions
Fe	Fe_3C	—	FeO, FeS
Si	—	Si_3N_4	SiO_2, (Fe,Mn)O–SiO_2, Al_2O_3–SiO_2, (Fe,Mn)O–Al_2O_3–SiO_2, CaO–Al_2O_3–SiO_2
Mn	—	—	(Mn,Fe)O, MnO–SiO_2, (Mn,Fe)S
P	—	—	—
S	—	—	Sulfides
Ni	—	—	—
Cr	Cr_7C_3 $Cr_{23}C_6$	Cr_2N	Cr_xO_y, (Fe,Mn)O–Cr_2O_3
Mo	Mo_2C, Mo_6C $Mo_{23}C_6$	Mo_2N	—
Ti	TiC	TiN	Ti_xO_y, (Fe,Mn)O–Ti_xO_y, TiO, TiS, Ti_3S_4 $Ti_4(C,N)_2S_2$
Zr	ZrC	ZrN	ZrO_2, ZrOS, ZrS, $Zr_4(C,N)_2S_2$
V	VC	VN	FeV_2O_4, V_2O_3, VO
Nb	NbC	NbN	$FeNb_2O_6$, NbO_2
Al	—	AlN	Al_2O_3, (Fe,Mn)O–Al_2O_3, CaO–Al_2O_3–Al_xON_y
Ca	—	—	CaO–Al_2O_3, CaO–Al_2O_3–SiO_2, CaS

EXPERIMENTAL PROCEDURE

Five commercial filler wires were used to submerged arc weld on a niobium microalloyed steel plate. The electrodes presented very different Mn/Si ratios and microalloying elements (Ti, Zr, Al) contents. The compositions of the base plate and the filler wires are given in Table II.

A CaF_2–CaO–SiO_2 flux was chosen to produce the welds. Previous work [15] showed that this system is very compatible for high strength low alloy (HSLA) steel welding, providing low oxygen content welds with

Table II. The Welding Parameters and Chemical Compositions of the Base Metals and the Welding Electrode Wires used in this Work

Current	310 A
Voltage	35 V
Travel Speed	4.4 mm/s
Heat Input	2.45 kJ/mm (62 kJ/in.)

Base Metal			Frostline[1]			Quest[1]
Flux			#13			OP121TT
Electrode	E70S3	E70SG	EH14	EM5K	TiBor22	TiBor22
Weld Designation	S313H	SG13H	EH13H	EM13H	Ti13H	TiOeH

	C	Mn	Si	P	S	Cu	Cr	Ni	Mo	Al	Ti	Zr	B[2]	V	Nb
Frostline	0.140	1.250	0.220	0.008	0.008	0.210	0.140	0.170	0.030	0.019	—	—	—	—	0.029
Quest	0.093	1.580	0.200	0.012	0.008	0.120	0.120	0.120	0.210	0.056	—	—	7	1	0.032
E70S3	0.124	1.152	0.560	0.021	—	0.070	—	—	—	0.010	—	—	—	—	—
E70SG	0.066	1.690	0.610	0.016	0.028	0.020	—	—	—	0.010	—	—	—	—	—
EH14	0.113	2.004	0.012	0.004	0.078	0.180	—	—	—	—	—	—	—	—	—
EM5K	0.036	1.169	0.446	0.008	0.016	0.020	—	—	—	0.100	0.083	0.065	—	—	—
TiBor22	0.058	1.480	0.035	0.008	0.006	0.770	0.117	0.100	0.330	0.028	0.031	—	70	—	—

	SiO_2	Al_2O_3	MgO	CaO	MnO	TiO_2	CaF_2	Na_2O	Fe_2O_3	C
OP121TT	10.7%	17.3%	31.0%	6.6%	1.1%	0.86%	24.1%	0.78%	1.9%	0.35%

NOTES:
(1) Commercial trade names of base metals.
(2) Boron concentration given in ppm, all other elements given in weight percent.

high volume fraction of acicular ferrite. The manganese, silicon, and niobium loss from the weld metal to slag can also be easily controlled. The composition of this flux system is indicated in Figure 2.

Single-v-grooved welds were made on strips of 380 mm × 110 mm × 13 mm (15 in. × 4.5 in. × 0.5 in.). In order to avoid the contamination of the weld joints by scales from flame cutting of the edges, mill scale or rust, the surfaces of the plates (besides the grooves) were also machined. The joint geometry is shown in Figure 3.

During the welding procedure, the parameters were controlled to obtain welds of heat input of approximately 2.5 kJ/mm. Values are given in Table II.

The chemical analyses of the welds were performed with a Baird Atomic Spectrovac Model 1000 Emission Spectrometer. Weld metal oxygen, nitrogen, and carbon content were determined using Leco Interstitial Analyzers. Macro and microhardness measurements were done on all the weldments.

Transverse sections were cut from the weldments and their surfaces prepared for quantitative metallography. Due to the extremely small sizes of the inclusions in the weld metal, attempts to characterize them (with respect to their size, number, and distribution) by light microscope were unsuccessful. Scanning electron microscope (SEM) and transmission electron microscope (TEM) works were, instead, carried out for inclusion determination. Carbon extraction replicas were obtained from the welds in order to examine the inclusions and other second phases present in the welds.

The replicas were mounted on aluminum studs as shown in Figure 4. Two layers of self-adhesive copper tapes were inserted between the replica and the aluminum holder so as to avoid the aluminum excitation from the holder, which may cause interference on the aluminum readings coming from the inclusions.

For the determination of the chemical composition of the inclusions, a Hitachi S415A SEM equipped with a Tracor Northern TN2000 and TN4000 EDS unit was used. The standardless semi-quantitative (SSQ) analysis program [16] was used for processing the electron beam excited X-ray fluorescence spectra. In this investigation, initial tests included the following chemical elements: Al, Si, P, S, K, Ca, Ti, V, Cr, Mn, Fe, Ni, Cu, Zr, Nb, and Mo. However, consistent negative results for K, Cr, Nb, Mo, Ni, and V were observed. Copper was excluded from the list because of the possible interference of the microscope components and the sample mounting procedure, as described previously. Therefore, only the remaining nine elements were requested in the final calculation subroutine for the inclusions identification.

In an attempt to identify the inclusions and characterize their crystalline nature, selected area diffraction (SAD) technique was used. In addition, acid extraction of nonmetallic particles was performed, and the collected residue was examined using a Philips X-ray diffractometer.

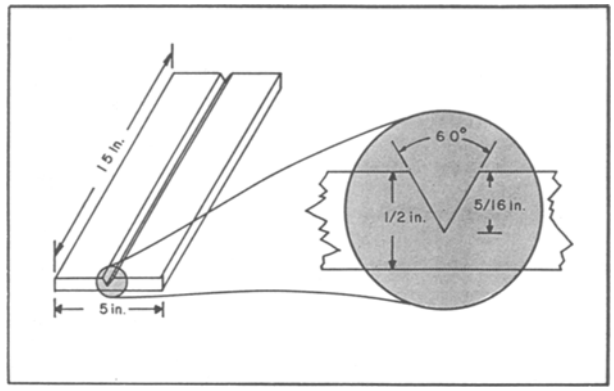

Fig. 3. Joint geometry of the single-v-grooved welds.

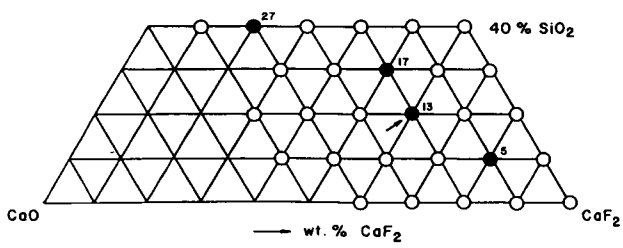

Fig. 2. Partial ternary diagram of CaF_2–CaO–SiO_2 system showing the nominal composition of the flux used in this work (flux number 13).

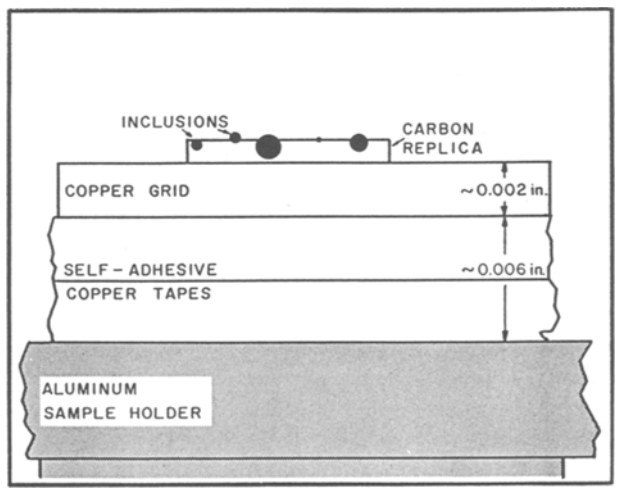

Fig. 4. Mounting sequence of a carbon extraction replica on an aluminum sample holder for EDS inclusion analysis.

RESULTS AND DISCUSSION

Manganese and Silicon Effect

As mentioned previously, manganese and silicon are deoxidizers and their concentration in the weld pool provide important information concerning the inclusion population. With increasing manganese content, oxygen was found to decrease, Figure 5. This indicates that manganese is indeed effective in deoxidizing the weld pool. Contrary to the manganese effect, increasing silicon concentration in the weld metal led to an increase of oxygen content, as shown in Figure 6. Similar trends were observed by other investigators [17–18]. The difference in behavior of oxygen in the weld metal described above can be related to the inclusion population. Recent literature showed that higher oxygen content welds usually contain a large number of small size inclusions of diameters less than 1.0 μm [19–23]. The fineness of the inclusions prevents the particles from being eliminated by flotation, due to low buoyancy force. However, part of the inclusions is separated from the weld pool by the convective motion of the liquid metal. The remaining part is trapped and affects the lower temperature solid state transformations. Fine austenite grains result with a final microstructure composed of high volume fraction of grain boundary ferrite and some acicular ferrite. Figure 7 is a light micrograph of weld S313H of high oxygen content and fine sized inclusions, with approximately 40% of acicular ferrite. Lower oxygen welds such as the one illustrated in Figure 8, TiOeH contain larger sized particles and coarser austenite grains. The final microstructure is observed to be very high in acicular ferrite content. The average particle size variation with weld metal oxygen is shown in Figure 9. By considering inclusions of size larger than 0.2 μm, the mean particle size was found to increase with the inclusion former's concentration. However, more careful metallographic evidences showed that inclusion size actually decreases with weld metal oxygen and sulfur concentration. This is not unreasonable, since higher concentration will increase the nucleation rate and will result in a larger number of smaller particles.

In the molten pool, silicon combined with oxygen to form silica or silicates. The total oxygen increase

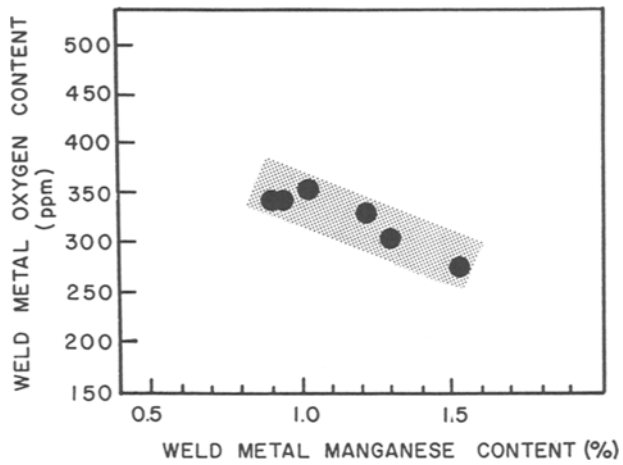

Fig. 5. Variation of weld metal oxygen content as a function of manganese concentration.

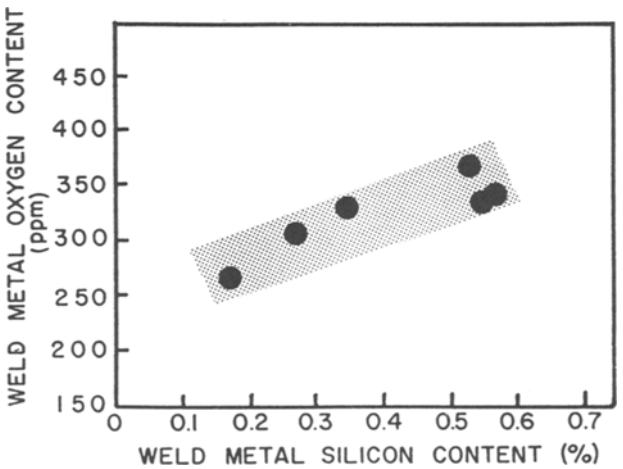

Fig. 6. Variation of weld metal oxygen content as a function of silicon concentration.

Fig. 7. Light micrograph of weld S313H of high oxygen content and fine sized inclusions. Notice the amount of grain boundary ferrite, widmanstatten ferrite, and ferrite aligned with carbide.

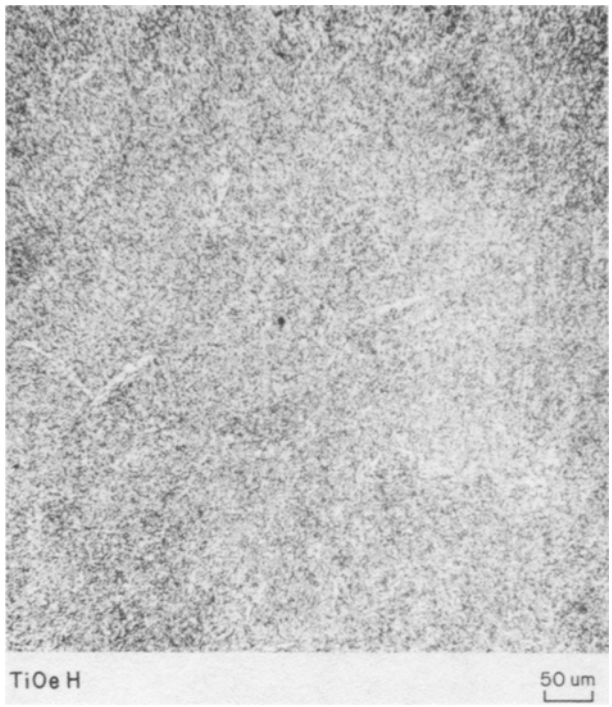

Fig. 8. Light micrograph of weld TiOeH of low oxygen content and large size inclusions. Notice the high volume fraction of acicular ferrite present.

with silicon seems to indicate that the deoxidation products were present and detected together with the acid soluble silicon. The decreasing oxygen content with an increase of manganese can also be related to inclusions' formation and their elimination from the weld pool. The presence of manganese in the weld decreased the inclusion population by promoting particle coalescence, since larger mean particle size was observed for higher manganese and lower oxygen welds. Combining the silicon and manganese effects observed, the following explanation seems to be reasonable. Conditions for the nucleation of silica and silicate particles are thermodynamically more favorable than for manganese oxide, and numerous particles are formed. With limited growth and coalescence, the fine particles will end up disseminated in the weld metal. This apparently justifies the observed increase of oxygen with increasing weld metal silicon content.

The description of nonmetallic inclusions as a function of manganese and silicon concentration seems to be adequate in a first analysis. It does not, however, take into account that the two elements coexist in the liquid metal pool. Actually, the ratio of manganese and silicon concentration will better express their combined effect on the weld metal oxygen and microstructure which is shown in Figure 10. An increase of Mn/Si ratio from one to nine reduced the weld metal oxygen from 350 ppm to 270 ppm. The effectiveness of deoxidizers such as manganese and silicon in oxygen control can be explained by the activity of silica in the molten weld pool. High Mn/Si ratio lowers the activity of silica which increases the deoxidizing power of silicon [5]. This results in more numerous particles being trapped in the weld pool. In order to obtain an inclusion population of correct size distribution for high volume fraction of acicular ferrite, the consumables (welding electrode and flux) that result in a high weld metal Mn/Si ratio should be selected. It should be reminded, however, that the hardenability effect of manganese and silicon cannot be overlooked.

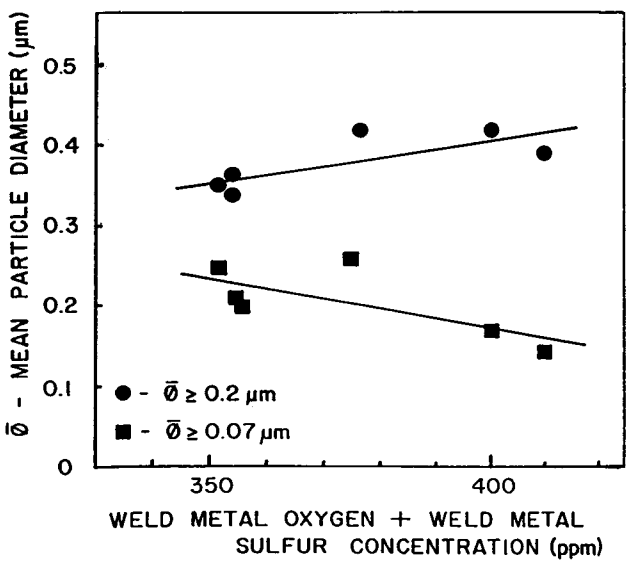

Fig. 9. Variation of mean particle size of the inclusions with weld metal oxygen and sulfur content.

Chemical Composition of the Inclusion

Chemical analysis of some of the particles extracted from the weld metals S313H and TiOeH are summarized in Tables III and IV. As can be seen in Figures 11 and 12, the chemical nature of the inclusions

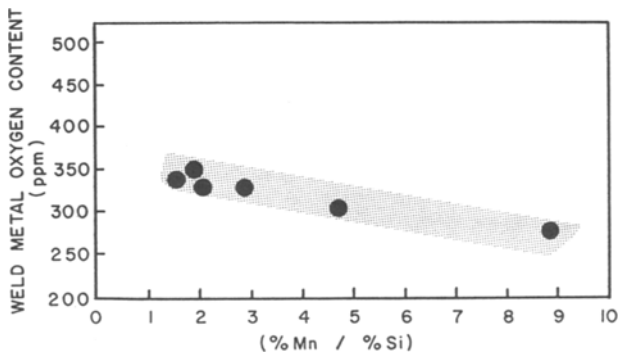

Fig. 10. Variation of weld metal oxygen content as a function of Mn/Si ratio (composition of Mn and Si expressed in weight percent).

Table III. Chemical Composition of Some Representative Inclusions Extracted from the S313H Weld Metal

Mn (%)	Si (%)	S (%)	Fe (%)	Al (%)	Ca (%)
57.5	3.7	27.0	9.3	2.7	0
57.2	6.7	36.0	0	0	0
46.7	15.6	22.7	10.7	4.2	0
44.9	13.6	22.5	14.0	5.0	0
41.9	9.5	27.6	21.1	0	0
37.8	35.4	8.4	10.1	8.4	0
36.5	46.6	7.5	0	9.5	0
34.9	37.6	18.2	0	9.2	0
33.0	41.5	11.0	7.2	7.5	0
21.2	71.9	0	0	7.0	0
10.6	16.7	9.6	63.1	0	0
0	80.1	0	20.0	0	0
0	72.8	0	0	27.2	0
0	66.8	0	19.9	13.3	0
0	52.8	20.9	26.3	0	0
0	30.3	0	8.9	61.0	0
0	26.7	0	7.2	66.1	0
0	25.1	0	68.4	4.5	2.0
0	12.9	3.7	83.5	0	0
56.0	7.7	25.4	8.6	2.4	0
53.3	6.1	29.8	8.4	2.1	0.5
51.5	5.9	27.6	12.8	2.3	0
49.3	12.9	25.7	8.3	3.9	0
47.8	15.0	25.5	8.6	3.1	0
47.5	36.9	15.6	0	0	0
46.9	6.1	30.1	8.7	8.2	0
45.8	7.0	32.6	9.5	5.3	0
40.8	15.9	33.2	7.9	2.3	0
40.6	13.8	31.6	9.8	4.3	0
39.9	40.2	8.2	5.9	5.8	0
38.4	39.8	7.3	9.2	5.3	0
37.0	36.8	17.5	0	8.7	0
36.0	34.4	17.3	6.3	6.2	0
35.8	18.5	36.0	9.8	0	0
35.6	47.1	8.5	0	8.8	0
33.7	32.0	27.0	0	7.3	0
33.6	13.3	12.9	36.6	3.7	0
30.9	47.0	5.2	10.3	6.7	0
29.3	31.3	23.8	7.2	8.4	0
22.5	39.8	25.3	12.5	0	0

Table IV. Chemical Composition of Some Representative Inclusions Extracted from the TiOeH Weld Metal.

Mn (%)	Si (%)	Al (%)	Fe (%)	Ti (%)	S (%)
42.7	7.3	21.0	0	9.9	19.1
46.2	1.0	29.9	0	2.1	20.9
48.7	5.2	17.9	0	2.3	26.0
19.0	17.1	19.3	29.3	0	15.4
27.3	9.2	47.3	5.2	2.8	8.3
24.1	7.7	55.7	4.0	6.2	2.4
25.7	18.7	40.4	0	8.8	6.4
40.5	0.9	36.8	5.3	1.8	14.7
22.0	7.2	45.9	6.1	15.6	3.2
27.5	3.9	56.0	3.9	6.7	2.0
50.5	3.5	12.5	8.4	0	25.0
25.8	11.7	49.1	5.6	4.5	3.3
25.4	1.0	61.7	3.8	7.4	0.8
28.0	10.8	44.3	4.4	9.4	3.1
34.4	5.1	37.1	5.4	5.1	13.0
54.0	1.8	5.6	7.4	0	31.4
0	19.8	66.6	10.2	0	3.5
21.8	15.5	38.9	8.4	11.5	4.0
27.0	4.6	56.6	4.4	5.2	2.3
25.9	8.0	44.4	6.3	13.1	2.4
34.9	6.0	36.8	5.7	10.4	6.2
0	72.3	0	27.8	0	0
16.6	38.0	23.2	0	17.9	4.5
20.3	29.5	34.9	0	10.5	4.9
25.4	14.0	45.0	5.1	0	10.5
10.5	43.5	39.2	6.9	0	0
29.8	4.4	58.8	0	3.9	3.1
24.6	4.2	59.0	4.3	6.3	1.7
29.5	8.3	36.8	6.7	6.4	12.5
0	63.9	7.9	28.2	0	0
45.2	4.3	27.3	0	2.5	20.8
27.6	6.4	55.9	4.6	3.3	2.2
30.5	5.0	48.9	9.0	5.2	1.5
29.5	8.2	27.6	12.5	5.4	17.0
17.5	11.1	60.7	7.8	3.0	0
42.0	3.8	30.5	0	6.4	17.3
26.3	13.7	36.3	0	23.7	0
35.7	4.0	36.4	5.1	1.8	17.1
28.4	4.8	54.5	0	4.6	7.7
0	38.5	42.9	18.6	0	0
31.1	69.0	0	0	0	0

is very complex and very large variations in manganese and silicon content were found.

Using stoichiometric calculations, chemical formulas were calculated for all inclusions analyzed. Diffraction analysis results to determine the chemical bonding nature of the inclusions will be reported later. More than 50 types of inclusions could be identified. The 12 major types are, in decreasing order of occurrence frequency,

1. $MnO–SiO_2–FeO–Al_2O_3$
2. $SiO_2–FeO–Al_2O_3$
3. $MnS–MnO–SiO_2–FeO–Al_2O_3$
4. $MnO–SiO_2–FeO–Al_2O_3–TiO_2$
5. $MnS–SiO_2–FeO$
6. $MnS–FeO–SiO_2–Al_2O_3$
7. $TiO_2–ZrO_2–Al_2O_3–MnO–P_2O_5$
8. $SiO_2–FeO$
9. $MnS–MnO–SiO_2–FeO$
10. $MnO–SiO_2–Al_2O_3$
11. $SiO_2–Al_2O_3$
12. $TiO_2–ZrO_2–Al_2O_3–SiO_2–MnO–P_2O_5$

Table V shows the other types of inclusions identified in this investigation, together with their occurrence in the different weld specimens. Inclusions extracted from S313H and SG13H welds exhibited the largest amount

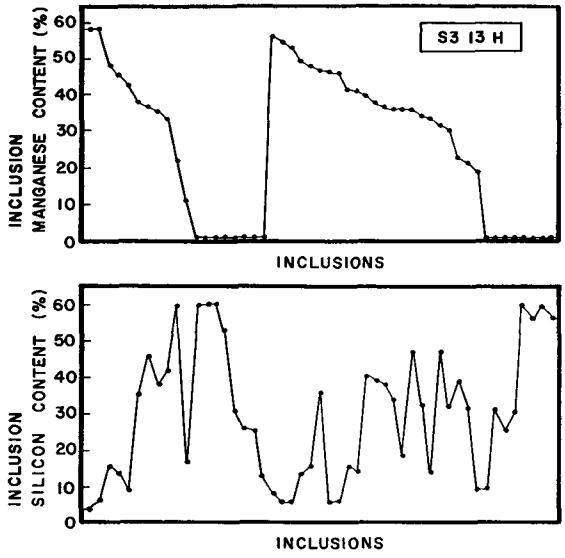

Fig. 11. Variation of manganese and silicon content in the inclusions extracted from S313H weld metal showing the complexity of the chemical nature of the inclusions.

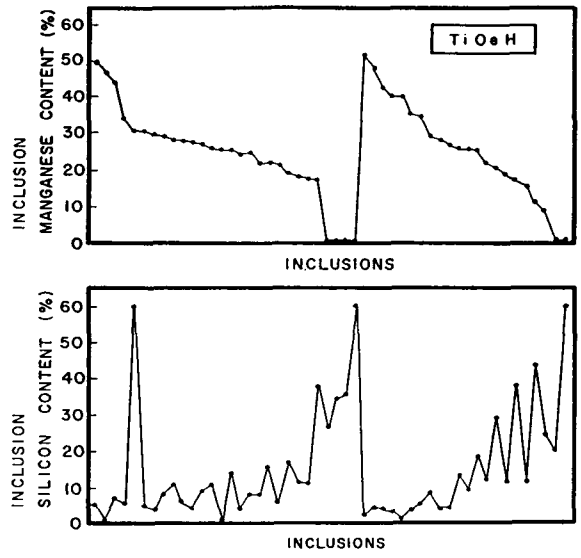

Fig. 12. Variation of manganese and silicon content in the inclusions extracted from TiOeH weld metal showing the same kind of complexity shown in Figure 11. Notice however, the overall related change of silicon with the concentration of manganese.

Table V. Summary of the Types of Inclusions Found in the Weld Metals Investigated. Types: (1) S313H, (2) SG13H, (3) EH13H, (4) EM13H, (5) Ti13H, (6) TiOeH.

Type	(1)	(2)	(3)	(4)	(5)	(6)	Type	(1)	(2)	(3)	(4)	(5)	(6)
MnS	—	6[1]	—	—	—	—	MnS–MnO–SiO_2–Al_2O_3–FeO–TiO_2	—	—	—	—	4	9
MnS–Al_2O_3	—	—	—	—	—	4	MnS–SiO_2–FeO–Al_2O_3–ZrO_2–TiO_2–P[2]	—	—	—	2	—	—
MnS–SiO_2	2	—	—	—	—	—	MnO–SiO_2	—	—	—	—	—	2
MnS–MnO	—	—	—	2	—	—	MnO–Al_2O_3	—	—	—	—	—	2
MnS–FeO	—	—	—	6	—	—	MnO–SiO_2–FeO	—	3	—	—	—	—
MnS–MnO–SiO_2	1	2	—	—	—	—	MnO–SiO_2–Al_2O_3	2	3	7	—	—	4
MnS–MnO–FeO	2	9	—	2	—	—	MnO–Al_2O_3–TiO_2	—	—	—	—	—	7
MnS–SiO_2–FeO	20	14	—	—	—	—	MnO–SiO_2–Al_2O_3–TiO_2	—	—	—	4	—	11
MnS–SiO_2–Al_2O_3	6	—	7	—	—	2	MnO–SiO_2–FeO–Al_2O_3	—	14	20	—	37	7
MnS–TiO_2–ZrO_2	—	—	—	2	—	—	MnO–SiO_2–FeO–Al_2O_3–TiO_2	—	—	—	2	16	13
MnS–MnO–Al_2O_3	—	—	—	—	—	2	SiO_2	—	—	—	—	4	2
MnS–MnO–SiO_2–FeO	6	11	—	—	2	—	SiO_2–FeO	14	6	—	—	2	2
MnS–MnO–SiO_2–Al_2O_3	6	9	—	—	4	—	SiO_2–FeO–P	—	—	—	—	2	—
MnS–FeO–SiO_2–Al_2O_3	12	3	—	2	4	2	SiO_2–Al_2O_3	2	—	7	10	—	8
MnS–FeO–SiO_2–TiO_2	—	—	—	2	—	—	SiO_2–FeO–Al_2O_3	16	—	33	4	8	11
MnS–MnO–TiO_2–Al_2O_3	—	—	7	—	—	2	SiO_2–TiO_2–Al_2O_3	—	—	—	2	—	—
MnS–FeO–Al_2O_3–TiO_2	—	—	—	2	—	—	SiO_2–Al_2O_3–CaO	—	3	—	—	—	—
MnS–MnO–FeO–TiO_2	—	—	—	2	—	—	SiO_2–Al_2O_3–FeO–FeS	—	—	—	—	2	—
MnS–MnO–FeO–Al_2O_3	—	—	—	—	—	5	SiO_2–FeO–Al_2O_3–TiO_2	—	—	7	2	—	—
MnS–FeS–SiO_2–Al_2O_3–FeO	—	—	—	—	2	—	FeO–Al_2O_3	—	—	7	—	—	—
MnS–TiO_2–FeO–Al_2O_3–SiO_2	—	—	—	2	—	—	TiO_2–ZrO_2–Al_2O_3–MnO–P	—	—	7	22	—	—
MnS–TiO_2–ZrO_2–FeO–Al_2O_3	—	—	—	4	—	—	TiO_2–ZrO_2–FeO–Al_2O_3–MnO–P	—	—	—	6	—	—
MnS–MnO–SiO_2–FeO–Al_2O_3	10	14	7	—	16	5	TiO_2–ZrO_2–Al_2O_3–SiO_2	—	—	—	2	—	—
MnS–MnO–SiO_2–Al_2O_3–TiO_2	—	—	—	—	—	4	TiO_2–ZrO_2–Al_2O_3–SiO_2–MnO–P	—	—	—	10	—	—
MnS–SiO_2–FeO–Al_2O_3–TiO_2	—	—	—	—	—	2	TiO_2–ZrO_2–FeO–Al_2O_3–SiO_2–MnO–P	—	—	—	6	—	—

NOTES:
(1) Number data represent occurrence frequency in percent.
(2) P—assumed to be P_2O_5 present in the inclusions.

of sulfur, iron, silicon, and manganese, in the combined form of manganese sulfide, manganese oxide, silicon dioxide, and iron oxide.

Inclusion Chemical Composition and Weld Metal Microstructure

Metallographic analysis of Figures 7 and 8 showed that the S313H weld microstructure was composed mainly of primary ferrite (approximately 50% and acicular ferrite while TiOeH is an excellent weld because less than 10% primary ferrite could be observed. Figure 13 is a comparative chart showing the differences between the inclusion compositions of these two welds. Four elements (Si, Al, Fe, and S) were observed to be significantly different. Inclusions from the coarse microstructure weld (S313H) contained about 30% of silicon, 5% of aluminum, 15% of iron, and 15% of sulfur. The higher silicon content here observed supports the idea that much of the product of silicon reacting with oxygen is trapped in the weld metal. No detectable amount of titanium could be observed in the inclusions in this weld. For the fine microstructure weld, analyses of the extracted inclusions indicated approximately 15% of silicon, 30% of aluminum, less than 5% of iron, and also less than 5% of sulfur. In this case, the weld metal contained higher manganese and lower silicon, therefore the inclusions were also expected to contain less silicon. They also contained about 5% of titanium. The aluminum and iron content in the inclusions are good indicators of the state of deoxidation of the weld pool. The presence of a higher concentration of iron in the inclusions (in the form of FeO or FeS) actually indicates that the deoxidants added are insufficient to refine the molten steel. Consequently, hardenability agents such as manganese, chromium, and molybdenum will be depleted by oxidation, resulting in a coarser weld metal microstructure. Oxygen would not have reacted with iron to a great extent, as long as other deoxidants were present. A well-deoxidized weld pool usually provides better conditions for the recovery of elements such as titanium, boron, and aluminum, which are reported to be promoters of acicular ferrite [24–27]. As suggested by Pargeter [28], Keville and Cochrane [29], and Cochrane, Ward, and Keville [30], microstructures consisting largely of acicular ferrite were often seen associated with alumina rich inclusions. Figure 14 was constructed to verify the observation. Volume fraction of acicular ferrite was observed to increase with increasing inclusion aluminum content. At low inclusion aluminum contents, however, the correlation was not as clear. Acicular ferrite content varied from 20% to 80%. This agrees with the correlation proposed in the literature [31–33]. Figure 15 showed that a good correlation between inclusion and weld metal aluminum content was observed. By increasing the weld metal aluminum content, the inclusion aluminum content increased. This is reasonable because of the low

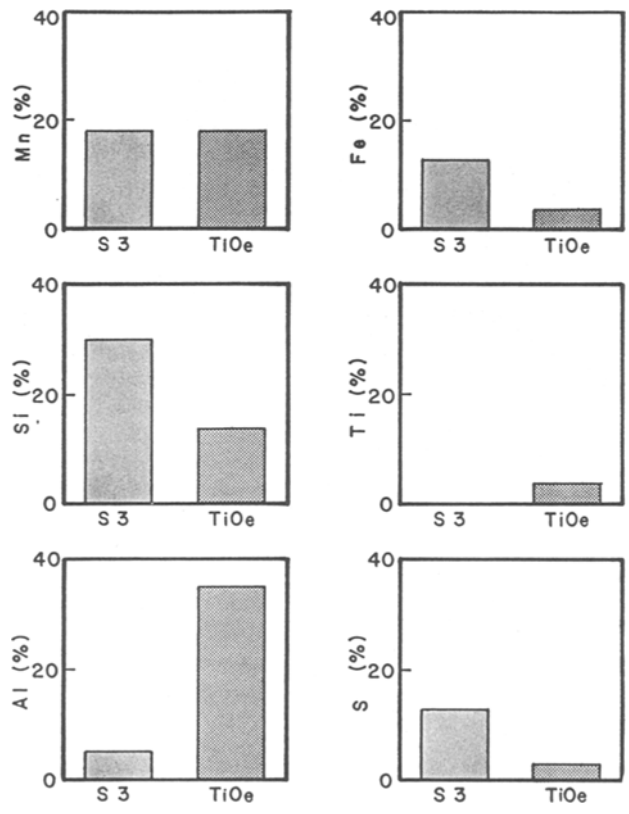

Fig. 13. Comparative chart showing the difference between the compositions of the inclusions extracted from S313H and TiOeH weld metals.

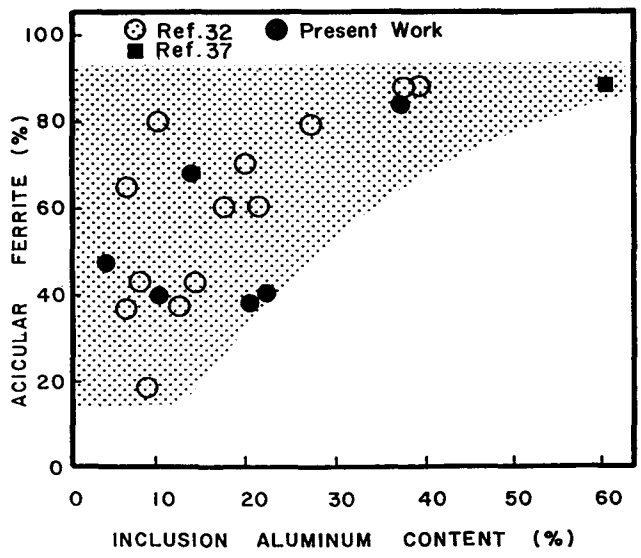

Fig. 14. Volume fraction of acicular ferrite as a function of inclusion aluminum content.

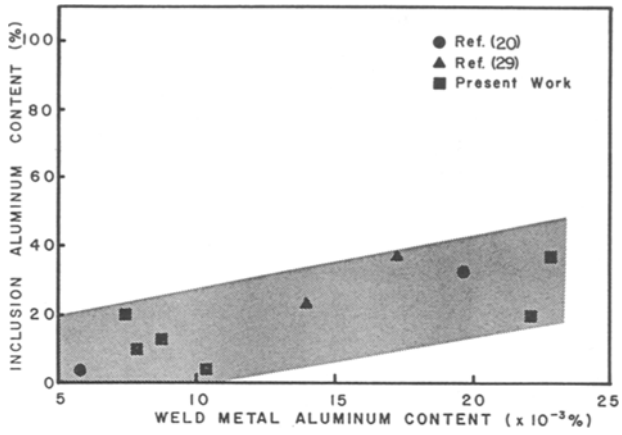

Fig. 15. Variation of inclusion aluminum content with weld metal aluminum content.

solubility of aluminum in iron, and its high affinity with oxygen.

Previously, Brownlee [34] reported that the final weld microstructure is determined by the presence of aluminum through its control of the inclusion size distribution and number density. Aluminum bearing inclusions tend to cluster and form larger particles, thus decreasing the overall number of oxide inclusions in the matrix. Since 87% of the inclusion investigated in the TiOeH weld contained aluminum, it is logical to suggest that clustering is very important in inclusion size control. Conversely, since only 55% of the inclusion in the S313H weld contained aluminum, then the non-agglomerating one will also play an important role in inclusion size distribution.

To determine the sulfur effect on weld metal phase transformation, volume fraction of acicular ferrite was plotted as a function of the inclusion sulfur content in Figure 16. When inclusion sulfur content was reduced to less than 10%, acicular ferrite increased. This agrees with the general observation that sulfur is harmful to the weld metal properties with respect to the promotion of coarse grain boundary ferrite.

Other investigators reported that sulfur usually occurs in the form of a surface layer on larger inclusions of silicates [35–37]. Many mechanisms were proposed to explain the effect of this sulfide layer inhibiting acicular ferrite nucleation. In the present research, no STEM work was carried out to characterize the microchemistry of the nonmetallic particles. However, the layering phenomenon was observed with both SEM/EDS and TEM extraction replica as shown in Figures 17 and 18. In addition, sulfur was found to exist in the form of α-MnS. Dispersement of fine α-MnS crystallites were found around the larger particles, as shown in Figure 19. Originally, MnS particles were thought to be associated with acidic fluxes. In

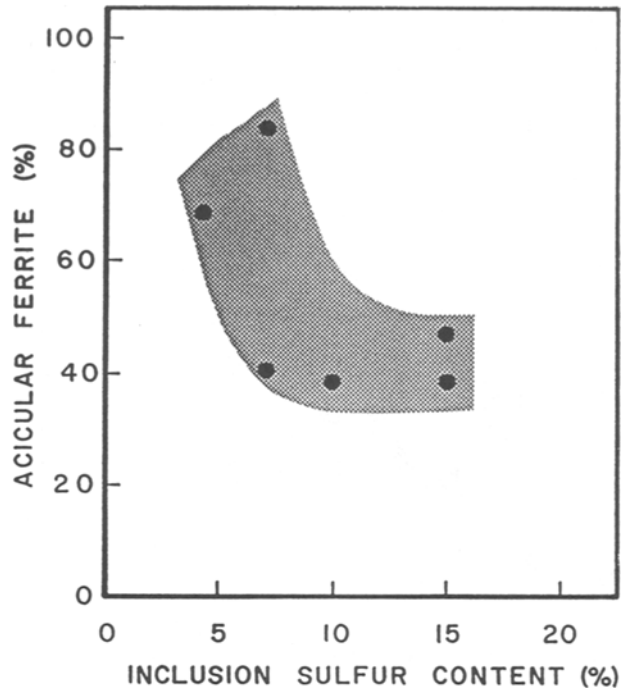

Fig. 16. Effect of inclusion sulfur content on the volume percentage of acicular ferrite in the final microstructure.

the present investigation, the flux was basic in nature (including CaF_2 as a basic component). This indicates that the definition of Basicity Index is incomplete and needs to be revised. In addition, the behavior of flux and weld pool interaction needs to be further illucidated.

The effects of weld pool deoxidation on hardenability element recovery could also be observed in the

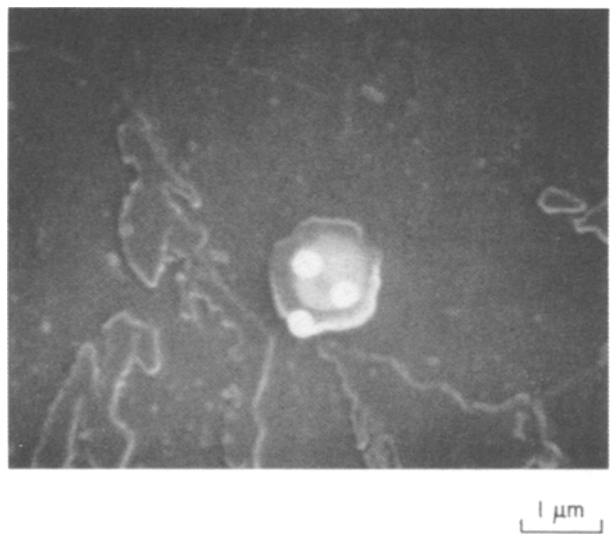

Fig. 17. SEM micrograph showing a layered inclusion with three white spots indicating the locations hit by the electron beam during the EDS analysis.

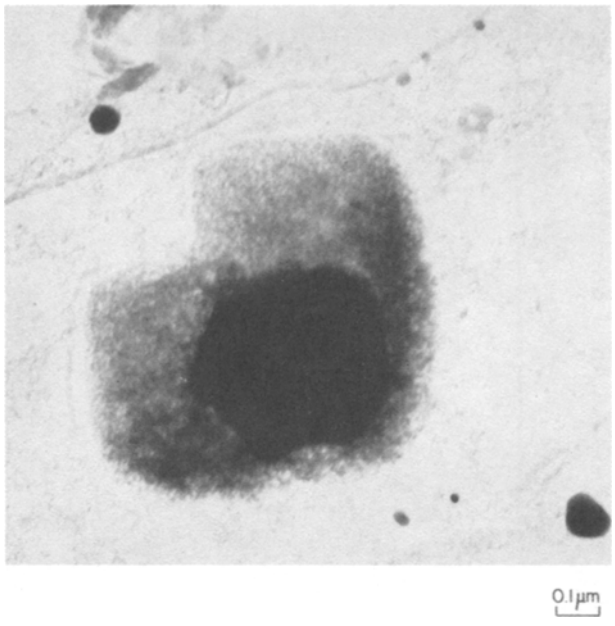

Fig. 18. TEM micrograph showing a layered inclusion.

calculation of delta managanese and delta molybdenum in the specimens Ti13H and TiOeH. Delta quantity is defined as the difference between the composition of a particular element determined analytically and the amount of that element which would be present if no elemental transfer from the weld pool to the flux or vice-versa had occurred. A negative value of delta means that during welding that particular element has been transferred from the weld metal to the slag, while a positive delta would indicate the element going from the molten flux to the weld metal. Delta molybdenum was determined to be −0.1573 and −0.0131 wt% for Ti13H and TiOeH, respectively. Comparing with the nominal molybdenum contents, one notices that the loss of molybdenum in the Ti13H weld was almost 100%. Delta manganese showed the same trend as molybdenum, −0.39 wt% in Ti13H weld and zero loss in TiOeH weld. Calculation also showed that boron loss in Ti13H was more significant than in the TiOeH weld. The lack of protection against oxidation with lower initial manganese content in the welding flux and base metal and in the Ti13H weld pool are the main reasons for the high losses of molybdenum and boron. The higher iron oxide content in the inclusions extracted from Ti13H as compared to that of TiOeH weld, was also an evidence of the lower degree of deoxidation in the weld pool.

Fig. 19. TEM micrograph showing the presence of small α-MnS inclusions around a larger oxide particle.

Weld Metal Inclusions: Crystalline or Glassy

Most of the inclusions observed were spherical in shape indicating their origin from the liquid state of the weld pool. Nevertheless, distinct geometrical shapes such as triangular, square, pentagonal, and hexagonal were also seen. In S313H, SG13H, EH13H, EM13H, and Ti13H welds, less than 5% of the inclusions were nonspherical. TiOeH weld showed approximately 12% shaped inclusions with square and hexagonal ones predominating over the other shapes. The importance of the inclusions in nucleating acicular ferrite could be clearly seen in Figure 20. From each one of the faces of the five-sided inclusion, an acicular ferrite lath was nucleated. This structure resembles that of a star and could be called "ferrite star." It seems to indicate that crystallography can exercise some influence on acicular ferrite nucleation through lower interfacial energy. This situation is not unique. Acicular ferrite was also observed to nucleate and grow out from spherical inclusions. Nevertheless, macroscopically observed smooth "spherical" surfaces may also show ledges and facets, Figure 21, indicating some signs of crystallinity.

Selective area diffraction was performed on the replica extracted particles. The bigger ones did not show diffraction pattern. Again, this does not preclude the possibility of the larger inclusions being crystalline. The reason for not obtaining diffraction pattern could be due to the size of the particles, being too thick for electron diffraction to occur. For the smaller particles (<0.07 μm) shown in Figure 19, a diffused ring pattern was obtained and shown in Figure 22. When the interplanar spacings were calculated, and the ratios between the planes determined, the small particles were

Fig. 20. Acicular ferrite laths nucleated and grown out of an inclusion.

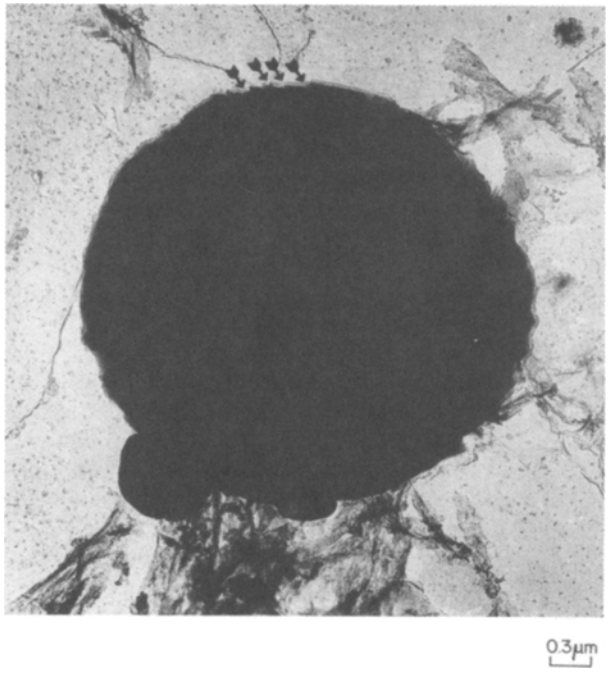

Fig. 21. TEM micrograph of a large inclusion showing ledges and facets suggesting a crystalline nature.

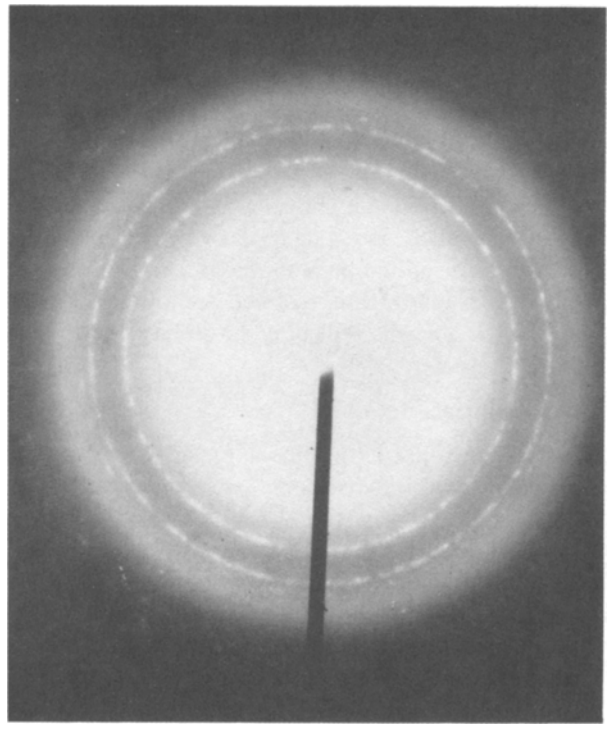

Fig. 22. Diffused ring pattern obtained in the SAD (selected area diffraction) analysis of the small α-MnS particles shown in Figure 20.

found to be face-centered cubic α-MnS with a lattice parameter equal to 5.248 Å.

Inclusions obtained from the weld samples using the acid extraction technique, as described previously, were examined using the Philips X-ray diffractometer. No diffraction pattern could be obtained. However, this is not conclusive in the determination of whether the particles are crystalline or amorphous. The extremely small quantity of residue collected could be insufficient for the characterization. Very fine powder could also cause problems in the X-ray diffraction procedure.

In the determination of whether the inclusions extracted were glassy or crystalline, chemical stoichiometry of the particles should also be considered. Crystals usually have well defined chemical compositions, while glassy inclusions may have their compositions varied between wide limits. Results from the present work showed that this might be the case. Within the same type of inclusions, wide composition variation was indeed observed. Again, this alone is not enough to conclude that the inclusions were glassy. Layered inclusions were observed, as illustrated previously. Especially in Figure 17, the three white spots on the inclusion were the points hit by the electron beam during the EDS analysis. The inner core was determined to be MnS, and the surface layer man-

ganese silicate. In the case of analyzing these particles, especially finer sized ones, often the thin surface films cannot be detected separately from the cores, and the compositions are reported as an average value leading to the impression of a wide composition variation.

From what is shown above, no definitive evidence could be supplied to characterize whether the inclusions were crystalline or amorphous. And in order to solve this problem, more refined techniques such as STEM microanalysis will have to be used.

CONCLUSIONS

The major results of this investigation can be summarized in the following conclusions:

1. Inclusion chemical composition is intimately related to the chemical composition of the consumables and base metal used.
2. Weld pool protection determines the amount of alloying elements recovered in the weld pool and the amount and composition of nonmetallic inclusions.
3. The effects of manganese and silicon on the total weld metal oxygen are opposite. Manganese lowers weld metal oxygen concentration. Contrarily, due to the entrapment of fine sized particles, silicon gathers and retains oxygen in the weld metal.
4. The major difference in inclusions for high and low oxygen weld systems are the silicon, aluminum, iron, titanium, and sulfur content. For high volume fraction of acicular ferrite, high inclusion aluminum and titanium content are required. Low silicon, iron, and sulfur are also important to obtain a refined weld metal microstructure.
5. Special techniques need to be devised to study the chemical structural nature of the inclusions to characterize their formation mechanism.

ACKNOWLEDGEMENT

The authors acknowledge the research and fellowship support of the United States Army Research Office, the Conselho Nacional de Pesquisa e Desenvolvimento do Brasil, and the material and equipment support of Lukens Steel Company and Hobart Brothers Company.

REFERENCES

1. R. Kiessling, "Non-Metallic Inclusions in Steel. Parts I–IV," London, The Metal Society, 1978.
2. L.G. Twidwell, "Physical Chemistry of Iron and Steelmaking," Butte, Montana College of Mineral Science and Technology.
3. U.S. Steel Corporation "The Making, Shaping, and Treating of Steels," 9th Edition, Pittsburgh, U.S. Steel Corporation, p. 281, 1971.
4. E.T. Turkdogan, "Deoxidation of Steel," *Journal of The Iron and Steel Institute*, 1972, v. 12, p. 21.
5. O. Grong, T.A. Siewert, G.P. Martins, and D.L. Olson, "A model for the sequence of reactions occurring during silicon-manganese deoxidation of mild and low alloy steel weld metals." Submitted for publication.
6. N.E. Hannerz and T. Werlefors, "The Influence of Parent Material Aluminum Content on Microstructure, Inclusion Distribution, and Mechanical Properties of Submerged Arc Weld Metal" in Proc. Intl. Conf. on *"Trends in Steels and Consumables for Welding,"* London, The Welding Institute, p. 335, 1978.
7. K. Narita, "Observation, Identification and Determination of Nonmetallic Inclusions and Precipitates in Steel," *Trans. ISIJ*, 1976, V. 16, p. 208.
8. I. Taguchi, "Inclusion Analysis of Steel Samples" in Proc. Symp. on *"Analysis of Ferrous and Non-Ferrous Metals,"* Peking, 1980.
9. F. Kurosawa, I. Taguchi, M. Tanino, H.G. Suzuki, and R. Matsumoto, "Observation and Analysis of Precipitates Formed in Steels at Elevated Temperatures using the Non-Aqueous Electrolytic-Potentiostatic Etching Method," *Journal of Japan Institute of Metals*, 1981, V. 45, p. 72.
10. P.H. Salmon Cox, and J.A. Charles, "Further Observations on the Analysis and Distribution of Non-Metallic Inclusions in a 0.2% C Steel Ingot," *Journal of The Iron and Steel Institute*, 1965, v. 5, p. 493.
11. S.E. Lunner, "Origin and Types of Slag Inclusions in Non-Stabilized Austenitic Acid Resistant Steel," *Journal of The Iron and Steel Institute*, 1972, v. 12, p. 168.
12. A.S. Venkatadri, "Mechanisms of Formation of Non-Metallic Inclusions in Aluminum-Killed Steels," *Trans. ISIJ*, 1978, V. 18, p. 591.
13. B. Ahlblom, H. Bergstrom, N.E. Hannerz, and I. Werlefors, "Influence of Welding Parameters on Nitrogen Content and Microstructure of Submerged Arc Weld Metal" in Proc. Intl. Conf. on *"The Effects of Residual, Impurity and Micro-alloying Elements on Weldability and Weld Properties,"* London, The Welding Institute, Paper 38, 1983.
14. R.C. Cochrane, J.L. Ward, and B.R. Keville, "The Influence of Deoxidation and/or Desulphurisation Practice on the Weld Metal Toughness of High Dilution Welds" in Proc. Intl. Conf. on *"The Effects of Residual, Impurity and Micro-alloying Elements on Weldability and Weld Properties,"* London, The Welding Institute, Paper 16, 1983.
15. S. Liu, C.B. Dallam, and D.L. Olson, "Performance of the CaF_2-CaO-SiO_2 system as a submerged arc welding flux for a niobium based HSLA steel" in Proc. of ASM Intl. Conf. on *"Welding Technology for Energy Applications,"* Gatlinburg, Tenn., p. 445, 1982.
16. J.H. Doyle, "ZAG 80: An improved Quantitative Analysis for the Flextran Language Systems," Rockwell Int. Report, RFP-3215, Rocky Flats Plant, Golden, Co., 1981.
17. D.J. Widgery, "New ideas on Submerged Arc Weld-

ing" in Proc. Intl. Conf. on *"Trends in Steels and Consumables for Welding,"* London, The Welding Institute, p. 217, 1978.
18. B.A. Graville, "Factors affecting the Toughness of Submerged Arc Weld Metal—Part II," *Technology Focus* (Welding Institute of Canada), V. 2, p. 1, 1980.
19. C.B. Dallam, S. Liu, and D.L. Olson, "Flux composition dependence of microstructure and toughness of submerged arc HSLA weldments," *Welding Journal,* 1985, 64(5): pp. 140-s–151-s.
20. P.L. Harrison, and R.A. Farrar, "Influence of oxygen-rich inclusions on the austenite to ferrite phase transformation in high-strength low-alloy (HSLA) steel weld metals," *Journal of Materials Science,* 1981, vol. 16: p. 2218.
21. M. Ferrante, and R.A. Farrar, "The role of oxygen rich inclusions in determining the microstructure of weld metal deposits," *Journal of Materials Science,* 1982, vol. 17, p. 3293.
22. S. Liu and D.L. Olson, "The Role of Inclusions in Controlling HSLA Steel Weld Microstructures," *Welding Journal,* 1986, vol. 65(6); pp. 139-s–150-s.
23. J.W. Jang, S. Shah, and J.E. Indacochea, "Influence of SAW Fluxes on Low Carbon Steel Weld Microstructure" in Conference Proceedings *ASM Materials Week '85,* Toronto, Canada, 1985.
24. S. Kanazawa, A. Nakashima, K. Okamoto, and K. Kanaya, "Improvement of weld fusion zone toughness by fine TiN," *Transactions ISTJ* 16, p. 486, 1976.
25. G.W. Heintze, and R. McPherson, "Grain refinement of steels by titanium innoculation during submerged arc welding," *Australian Welding Journal,* 1983, vol. 28, p. 37.
26. N. Mori, H. Homma, S. Okita, and K. Asano, "The behavior of B and N in notch toughness improvement of Ti-B bearing weld metals," IIW DOC IX-1158-80, 1980.
27. G.W. Heintze and R. McPherson, "Solidification Control of Submerged Arc Welds in Steels by Inoculation with Ti," *Welding Journal* 1986, Vol. 65(3): pp. 71s–82s.
28. R.J. Pargeter, *Investigation of Submerged Arc Weld Metal Inclusions.* The Welding Institute, Cambridge, England, 1981.
29. B.R. Keville and R.C. Cochrane, "Factors controlling the microstructure and toughness of submerged arc weldments" in Proc. 30th Annual Convention on *Welding Technology 82,* Hobart, The Australian Welding Institute, p. 263, 1982.
30. R.C. Cochrane, J.L. Ward, and B.R. Keville, "The Influence of deoxidation and/or desulphurisation practice on the weld metal toughness of high dilution welds" in Proc. Intl. Conf. on *"The Effects of Residual, Impurity and Micro-alloying Elements on Weldability and Weld Properties,"* London, England, The Welding Institute, Paper 16, 1983.
31. H. Terashima and P.H.M. Hart, "Effect of Flux TiO_2 and Wire Ti Content on Tolerance to High Al Content of Submerged Arc Welds made with Basic Fluxes" in Proc. Intl. Conf. on *"The Effects of Residual, Impurity and Micro-alloying Elements on Weldability and Weld Properties,"* London, The Welding Institute, p. 27, 1983.
32. M.E. Saggesse, A.R. Bhatti, D.N. Hawkins, and J.A. Whiteman, "Factors influencing inclusions chemistry and microstructure in submerged arc welds" in Proc. Intl. Conf. on *"The Effects of Residual, Impurity and Microalloying Elements on Weldability and Weld Properties,"* London, England, The Welding Institute, Paper 15, 1983.
33. R.A. Ricks, P.R. Howell, and G.S. Barritte, "The Nature of Acicular Ferrite in HSLA Steel Weld Metals," *Journal of Materials Science,* 1982, Vol. 17, p. 732.
34. J.K. Brownlee, Matlock, and G.R. Edwards, "Effects of Aluminum and titanium on the Microstructure and Properties of Microalloyed Steel Weld Metal" in Conf. Proceedings on *"Trends in Welding Research,"* ASM/AWS, Gatlinburg, Tenn., 1986.
35. L. Devillers, D. Kaplan, B. Marandet, A. Ribes, and P.V. Riboud, "The effect of low level concentrations of some elements on the toughness of submerged arc welded C–Mn welds" in Proc. Intl. Conf. on *"The Effects of Residual, Impurity and Micro-alloying Elements on Weldability and Weld Properties,"* London, England, The Welding Institute, p. 1, 1983.
36. G.S. Barritte, R.A. Ricks, and P.R. Howell, "Application of STEM/EDS to study of microstructural development in HSLA steel weld metals" in Proc. on *"Quantitative Microanalysis with High Spatial Resolution,* London, England, The Metals Society, p. 122, 1981.
37. E.S. Kayali, J.M. Corbett, and H.W. Kerr, "Observations on inclusions and acicular ferrite nucleation in submerged arc HSLA welds," *Journal of Materials Science Letters,* 1983, vol. 2, p. 123.